Defense Mechanism of Bioinspired Composites with Sinusoidally Periodic Helicoidal Fiber Architectures

Dianhao Chen[1]; Ruiheng Yang[2]; Weihua Guo[3]; Yao Huang[4]; T. X. Yu, Ph.D.[5]; and Sha Yin, Ph.D.[6]

Abstract: The fiber architectures of the stomatopod dactyl club lead to an effective toughening mechanism. Composites with sinusoidally periodic helicoidal (Herringbone-type) fiber architectures were fabricated using additive manufacturing and examined under dynamic loading. Under compression at different strain rates, stress distribution was found more uniform in the Herringbone-type structure than that in the Bouligand-type one because of fiber flattening. Under dynamic compression, Herringbone-type structures with amplitude gradients resisted large strains without significant damage, leading to greater energy absorption. Simulations indicated that the Herringbone-type structure mitigated the impact waves and facilitated uniform stress redistribution, whereas the Bouligand-type structure filtered the waves. These findings would shed light on the future designs of impact-resistant bioinspired materials. **DOI: 10.1061/(ASCE)AS.1943-5525.0001450.**

Author keywords: Mantis shrimp; Bioinspired composites; Architecture; Dynamic behavior; Crashworthiness.

Introduction

Many creatures have evolved various defense mechanisms for self-protection to adapt to the environment, such as camouflage, nocturnality, and protective armor (Quan et al. 2020; Meyers et al. 2008; Dunlop and Fratzl 2010). For example, extremely stiff, strong, and tough exoskeletons that can resist attack have evolved in crustaceans, including lobsters (Fabritius et al. 2009), crabs (Rosenberg 2002), and beetles (Zaheri et al. 2018). The dactyl clubs of the smasher-type peacock mantis shrimp (*Odontodactylus scyllarus*) can strike a target (e.g., hard-shelled and soft-bodied prey) with speeds up to 23 m/s and accelerations of >10,000 g, thus generating instantaneous forces of ~1,500 N without structural failure (Burrows 1969; Caldwell and Dingle 1975; Patek et al. 2004; Amini et al. 2014; Patek and Caldwell 2005).

To accomplish this feat, three different structural regions exist within the dactyl club of the mantis shrimp (Weaver et al. 2012; Yaraghi et al. 2016a; Amini et al. 2015; Grunenfelder et al. 2018). The inner periodic region, characterized by a Bouligand (twisted plywood) structure arising from alpha-chitin and amorphous calcium carbonate, serves as the primary energy-absorption region to prevent serious damage (Amini et al. 2014). The surrounding striated region, comprising highly aligned mineralized chitin fibrils, prevents excessive expansion and provides additional compressive and torsional stiffness during impact (Weaver et al. 2012). The outer impact region is a highly oriented and crystalline apatite mineral phase (i.e., fluorapatite colocalized with calcium sulfate) (Amini et al. 2014, 2015). Detailed investigations revealed the existence of a well-defined and highly ordered herringbone helicoidal structure, which enhances stress redistribution and out-of-plane stiffness and improves toughness by extending the path length of crack growth (Yaraghi et al. 2016a). Additionally, the helicoidal (Bouligand) architecture provides a shear-wave-filtering effect because of the existence of band gaps at frequencies related to the stress pulse generated by impact (Guarin-Zapata et al. 2015).

Bioinspired designs based on these complex architectures can be used to obtain strong and tough composite materials, which can be fabricated via additive manufacturing (Wu et al. 2020; Agarwal et al. 2018; Ren et al. 2018; Gu et al. 2016). Grunenfelder et al. (2014) fabricated carbon fiber–reinforced composites with a Bouligand structure and investigated the mechanical properties of the composites under impact loading (Grunenfelder et al. 2014). Yin et al. (2020) developed composites with the helicoidal architecture and discovered a novel mechanism that used fabrication defects, such as voids, to enhance impact toughness (Yin et al. 2020). Also, double-helicoidal composites inspired from coelacanth fish (Yin et al. 2021a), hollow honeytubes (Yin et al. 2019), hierarchical (Yin et al. 2013, 2018; Wu et al. 2019) and dual-phase lattices (Yin et al. 2021b; Guo et al. 2021) were also investigated to possess excellent energy-absorption capacity.

Wu et al. (2020) designed a discontinuous fibrous Bouligand architecture by combining the Bouligand structure of mantis shrimps and the nacreous staggered structure of abalones, and the architecture was found to support a hybrid toughening mechanism that enabled excellent fracture resistance with crack orientation insensitivity (Wu et al. 2020). Han et al. studied a novel composite laminate using basalt fiber with helical-sinusoidal bionic structure and found it possessing better impact resistance (Han et al. 2020). Yang et al. proposed a novel double-sine corrugated

[1]Dept. of Automotive Engineering, School of Transportation Science and Engineering, Beihang Univ., Beijing 100191, China.
[2]Dept. of Automotive Engineering, School of Transportation Science and Engineering, Beihang Univ., Beijing 100191, China.
[3]Dept. of Automotive Engineering, School of Transportation Science and Engineering, Beihang Univ., Beijing 100191, China.
[4]Dept. of Automotive Engineering, School of Transportation Science and Engineering, Beihang Univ., Beijing 100191, China.
[5]Professor, Dept. of Mechanical and Aerospace Engineering, Hong Kong Univ. of Science and Technology, Clear Water Bay, Kowloon, Hong Kong 999077, China.
[6]Associate Professor, Dept. of Automotive Engineering, School of Transportation Science and Engineering, Beihang Univ., Beijing 100191, China (corresponding author). ORCID: https://orcid.org/0000-0001-7061-1323. Email: shayin@buaa.edu.cn

Note. This manuscript was submitted on November 29, 2021; approved on March 10, 2022; published online on May 18, 2022. Discussion period open until October 18, 2022; separate discussions must be submitted for individual papers. This paper is part of the ***Journal of Aerospace Engineering***, © ASCE, ISSN 0893-1321.

sandwich structure, which significantly improved structural crashworthiness (Yang et al. 2017).

However, the toughening mechanism and dynamic mechanical properties of the herringbone helicoidal architecture in the impact region of the dactyl club of mantis shrimps have not been fully studied, especially under dynamic impact loading. In this study, a sinusoidally periodic helicoidal architecture based on the impact region of the appendage was designed, and the composites were fabricated using three-dimensional (3D) printing. Then, compression tests at different strain rates were conducted, and the results were compared with those for the Bouligand structure of the inner periodic region. Finally, wave filtering was investigated using finite-element analysis, and the effects of critical geometrical parameters and fiber architecture were analyzed to provide insights for the design of impact-resistant composite materials.

Materials and Methods

Design and Fabrication

Bioinspired composites with a helicoidal structure based on the herringbone microstructure in the impact region of stomatopod dactyl clubs were fabricated to examine the toughening mechanism and dynamic mechanical properties of this intricate microstructure. The results were expected to provide useful information for the manufacture of materials with great crashworthiness. Sinusoidally periodic fibers were constructed with and without an amplitude gradient, which were denoted as Herringbone_grad and Herringbone-type, respectively. The bioinspired helicoidal composites were printed using a multimaterial printing approach (STRATASYS J750, Stratasys, Edina, Minnesota). Cylindrical samples for compression were all printed layer by layer from the bottom to the top, with diameter D of 35 mm [Fig. 1(b)].

VeroPureWhite and Agilus30 FLX985 were selected as fibers and matrix, respectively. VeroPureWhite was over three orders of magnitude stiffer than Agilus30 FLX985, which was similar to the mechanical relationship of fibers and matrix in the stomatopod's appendage (Yaraghi et al. 2016b). Additionally, composites with helicoidally stacked straight fibers (Bouligand-type) were also fabricated for comparison with almost the same fiber volume fraction (0.27 for Herringbone_grad and Herringbone-type, and 0.29 for Bouligand-type). For the Herringbone_grad sample, the sinusoidal amplitude of each layer varied from 1.5 to 1 mm with a uniform gradient of 0.1 mm per layer. All the geometrical parameters are summarized in Table S1.

Mechanical Testing

Dynamic Compression of Bioinspired Composites

The quasi-static compression tests were carried out using an Instron 8801 (Norwood, Massachusetts) at a constant loading speed of 1 mm/min (a strain rate of $\sim 10^{-3}/\mathrm{s}$) at room temperature. Samples of each type were coated with paint to obtain a random

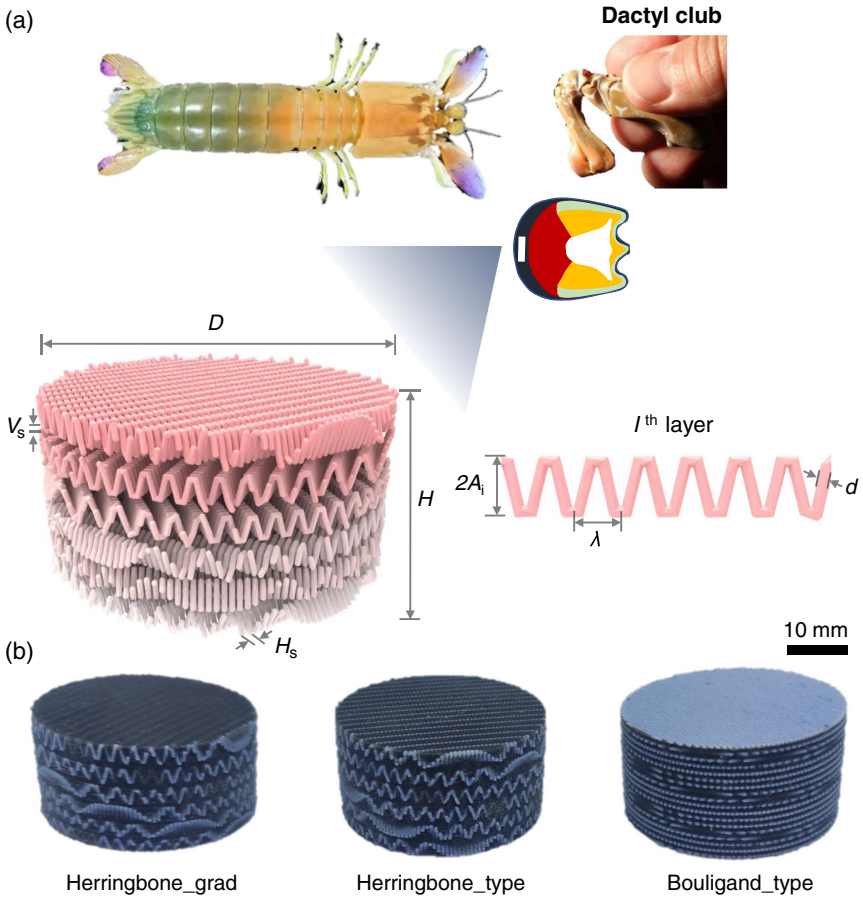

Fig. 1. (a) Geometrical illustration of the bioinspired sinusoidally periodic helicoidal (herringbone type) fiber architecture [reprinted from Yin et al. 2020, under Attribution 4.0 International (CC BY 4.0) license (https://creativecommons.org/licenses/by/4.0/)]; and (b) three types of 3D-printed samples: Herringbone_grad, Herringbone-type, and Bouligand-type.

J. Aerosp. Eng., 2022, 35(5): 04022056

black-and-white speckle pattern for posteriori digital image correlation (DIC) analysis. The intermediate-strain-rate dynamic compression tests were conducted using a Zwick HTM5020 (Ennepetal, Germany) with a constant loading speed of 2 m/s (~100/s) and 9 m/s (~500/s). The compression force and displacement were recorded using Zwick HTM5020 sensors. To visualize the deformation of the helicoidal composite samples, a high-speed camera (Photron SA1, Oho, Tsukuba, Japan) was used.

Elastic-Wave Propagation Tests

Wave propagation was characterized using a split-Hopkinson pressure bar (SHPB) testing system. The striker bar, which was accelerated by high-pressure gas in a gas gun, impacted the incident bar with a specific velocity of 5 m/s. Also, finite-element modeling was carried out and the simulation was validated using the experimental results to further elucidate the effects of geometry on the mechanical properties of the materials. The experimental setup and simulation details are provided in the Supplemental Materials.

Results and Discussion

Compressive Responses

Quasi-Static Compression

The engineering stress–strain curves and deformation patterns of the bioinspired helicoidal composites (i.e., Herringbone_grad, Herringbone-type, and Bouligand-type) under quasi-static compression were divided into three stages [Fig. 2(a)]: the linear-elastic stage (Stage I); the transition stage (Stage II) when cracks initiated and propagated; and the densification stage (Stage III) when stress increased rapidly. For the Herringbone-type and Herringbone_grad composites, the sinusoidal fibers near the compression plates were severely compressed and appeared to be flattened during Stage I. These fibers then separated from the matrix during Stage II, thus reducing the stiffness of the sample. Concurrently, cracks were initiated in the matrix and propagated through the middle layers, thus forming large cracks before densification [Fig. 2(a)].

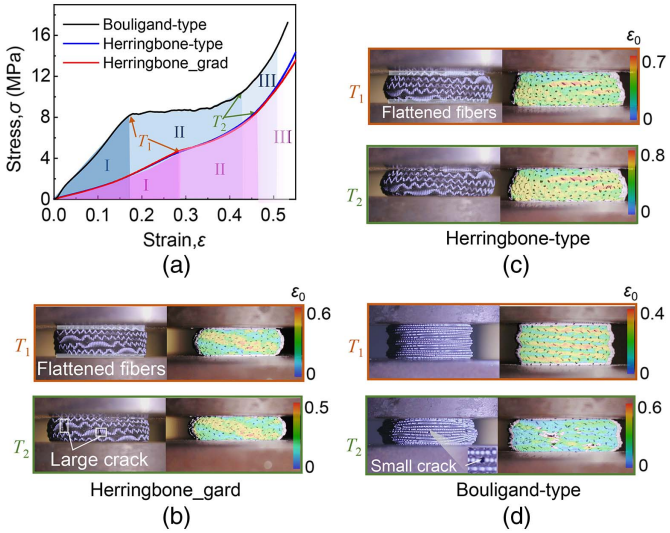

Fig. 2. Quasi-static compressive loading of the bioinspired samples: (a) compression stress–strain curves of three kinds of samples; and (b–d) deformation modes and corresponding strain contours of the Herringbone_grad, Herringbone-type, and Bouligand-type samples at the transition of the different stages. In plot (a), the three deformation stages (Stages I, II, and III) are marked under each curve. T_1 and T_2 represent the transition points of the different stages.

For the Bouligand-type composite, the representative stress–strain curves indicated that the samples were capable of absorbing energy during Stage II, which exhibited a steady stress plateau after the initial elastic stage and stress peak. Concurrently, several small cracks formed and propagated during Stage II. From the DIC results, the strain distribution was generally uniform in the Herringbone-type and Herringbone_grad composites, whereas a maximum strain zone was generated in each helicoidal (oblique) band of the Bouligand-type composites. Although designed with the same volume fraction, the amount of sinusoidally periodic fibers in the Herribone-type samples were far more less that of straight fibers in the Bouligand-type ones. Thus, the obtained stiffness and strength values of the sinusoidal ones were lower.

Intermediate-Strain-Rate Compression

The stress–strain curves and failure modes captured by the high-speed camera under intermediate-strain-rate compression are shown in Fig. 3. The mechanical properties including stiffness, densification strain, and energy absorption of the composites were determined. The energy absorbed before the densification strain (defined in Fig. S2) was calculated and is shown in Fig. 3. At the strain rate of 100/s, the herringbone samples absorbed more energy than the Bouligand-type samples; the former also exhibited postponed densification strain [Fig. 3(a)]. The absorbed energy values were about 11.54, 10.22, and 6.16 J/g for the Herringbone_grad, Herringbone-type, and Bouligand-type composites, respectively. Therefore, the herringbone structures were capable of withstanding large strains without significant damage, and the gradient architecture was beneficial for energy absorption.

At the strain rate of 500/s, the stiffness and strength values of the Herringbone-type samples were lower than those of the Bouligand-type samples [Fig. 3(b)], whereas the former ones possessed the greatest densification strain. Moreover, for the herringbone materials [Figs. 3(d and e)], the sinusoidally periodic fibers flattened and then expanded uniformly after the stress peak, thus mitigating the stress concentration.

Wave Filtering

The experimental and simulated results of elastic-wave propagation are shown in Fig. 4. In Fig. 4(a), the incident waves looked almost like rectangular pluses, whereas the reflection waves rose rapidly and then declined gradually until dropping abruptly to zero. The pulse signals were then transformed into the frequency domain using a fast Fourier transform (FFT) method (Yin et al. 2013). The existence of frequency band gaps in the bioinspired helicoidal structure was verified using a frequency response function (FRF)

$$X(f) = 20\log_{10}\frac{T(f)}{I(f)} \tag{1}$$

where $T(f)$ and $I(f)$ = amplitudes of the transmitted and incident wave signals obtained from the FFT analysis, respectively; and $X(f)$ = decibel (dB) value of the attenuated transmission of the signal. The four impulse transmission peaks, corresponding to the four band gaps, were significantly attenuated, as shown in Fig. 4(b). The stress waves and band gap distribution of the simulation results matched with those of the experimental results, thus validating the simulation.

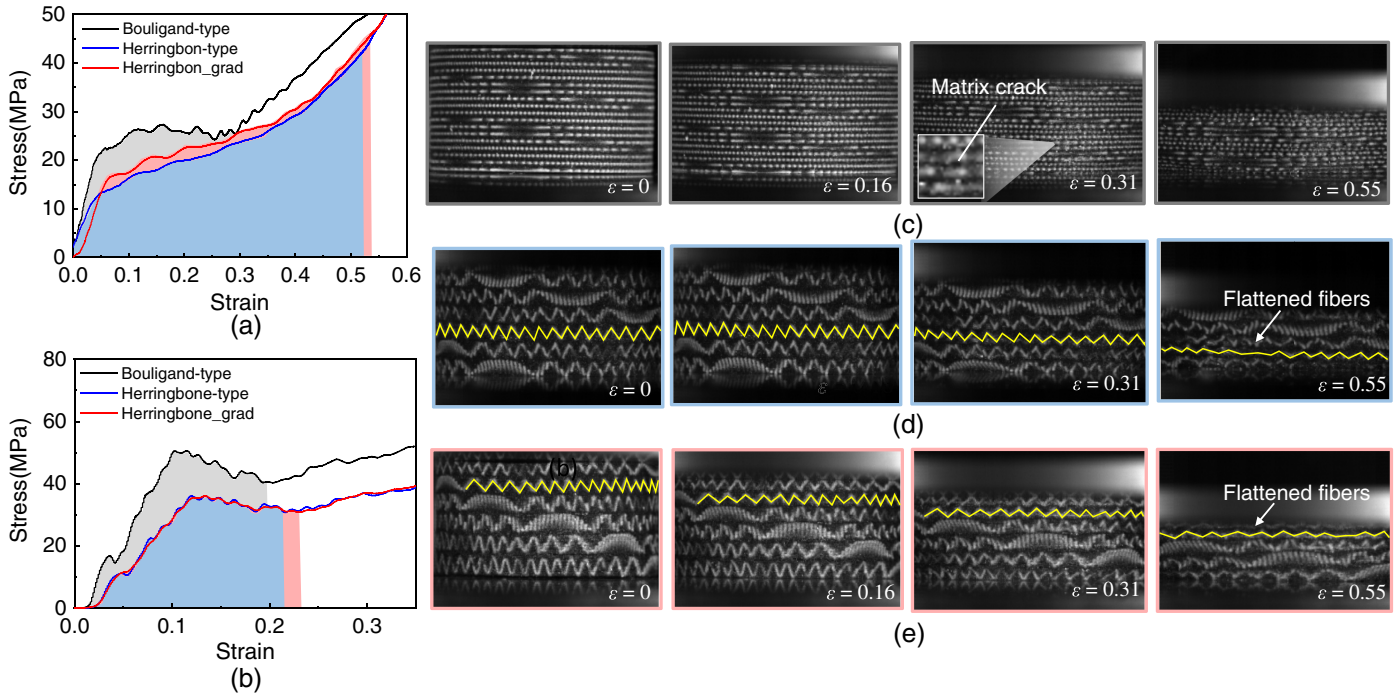

Fig. 3. Compressive stress–strain curves of the bioinspired samples under strain rates of (a) 100/s; and (b) 500/s; and deformation history of composites with (c) Bouligand-type; (d) Herringbone-type; and (e) Herringbone_grad structures under 500/s.

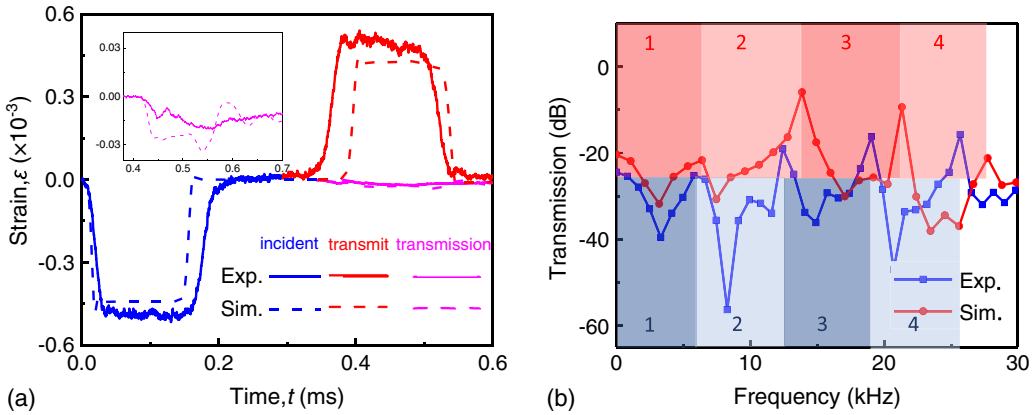

Fig. 4. Comparison of experimental and simulated results under SHPB system: (a) strain disturbance; and (b) impulse transmission.

Discussion

Mechanical Properties under Compression at Different Strain Rates

The strain-rate effect of stiffness for the parent material and the bioinspired composites with different architectures is shown in Fig. 5(a). The strength and energy-absorption variation were not considered here because of the monotonically increasing compressive characteristics. The stiffness increased with strain rate. At higher strain rates, the Herringbone-type and Bouligand-type composites were more sensitive than the Herringbone_grad composite.

To further uncouple the effects of fiber architecture, the effects of the parent materials (used for 3D printing of the composites) were investigated (detailed results are provided in the Supplemental Materials), and the effect of strain rate on the stiffness of the parent materials is included in Fig. 5(a). When the effect of fiber architecture was neglected, it was assumed that the stiffness of the composites was related to the stiffness and volume fraction of the parent materials, which were determined by using the following equation: $S_{\text{material}} = S_{\text{matrix}}\varphi_{\text{matrix}} + S_{\text{fiber}}\varphi_{\text{fiber}}$, where S_{matrix} and S_{fiber} are the stiffness, and φ_{matrix} and φ_{fiber} are the volume fraction of the matrix and fiber, respectively. A comparison of the stiffness variation between the bioinspired composites and parent materials effect indicated the existence of fiber architecture effect. In particular, the Bouligand-type architecture was more sensitive to strain rate.

Deformation Mechanism of Herringbone Architecture

The deformation mechanisms of the herringbone and Bouligand-type samples were analyzed, and the results are shown in Figs. 5(b and c). The fibers in the Bouligand-type structure deformed along the fiber direction under compression, so that

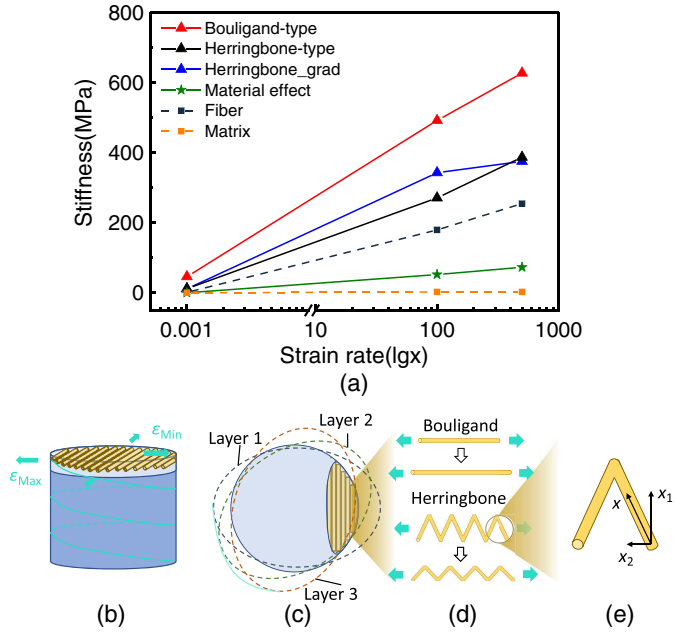

Fig. 5. (a) Stiffness variations of the bioinspired composites with different architectures and the parent materials used for 3D printing; and (b–e) schematic of the deformation mechanism of the bioinspired architectures. Plot (b) shows the helicoidal sample under compressive loading (spiral line represents the envelope curve of the maximum strain points of each layer), and plots (c–e) compare the deformation modes for each single fiber from the Bouligand-type and Herringbone-type fiber structures. X represents deformation along the fiber direction, and X_1 and X_2 are components in the horizontal and vertical directions that contribute, respectively, to fiber flattening and out-of-plane compressive stiffness.

the maximum strain of each layer rotated according to the helicoidal fiber architecture in the form of a spiral through the thickness [validated by DIC results in Fig. 2(b)]. However, for the fibers in the Herringbone-type structure, the deformation component along the thickness [Fig. 5(c)] contributed to compressive stiffness. Concurrently, the fibers extend and then flatten to distribute the stress uniformly. The fibers with amplitude gradients resisted stress fluctuation because of the interaction between the adjacent layers, which was enhanced by different flattened fibers. Fiber flattening and gradient effects were more pronounced in dynamic conditions, and as a result, the Herringbone_grad samples displayed better resistant capacity to impact than the other ones.

Effects of Geometrical Parameters

For the Herringbone-type composites with sinusoidally periodic fibers, three critical parameters (fiber amplitude A, wavelength λ, and helicoid angle α) were simulated to explore the effects of these geometrical parameters on dynamic stress–strain responses and stress-wave transmission. As shown in Fig. 6(a), the stiffness increased with fiber amplitude because fiber flattening was more difficult with greater fiber amplitudes. Moreover, transmission within the first band gap increased with fiber amplitude, and, as a result, wave filtering within the corresponding frequency range became weaker and thus the impact resistance of the structure decreased. However, transmission within the second band gap varied when the fiber amplitude was larger than 0.9 mm. In the last two band gaps, the transmission of 1.2 mm was greater than others, whereas the transmission was similar when the fiber amplitude was smaller than 1.2 mm. Therefore, the fiber amplitude mainly affects the first two band gaps at a relatively low frequency range and has limited influence on wave transmission at the high frequency range.

The stiffness decreased rapidly with an increase in the fiber wavelength λ [Fig. 6(b)], and this effect was pronounced for $\lambda < 6$ mm.

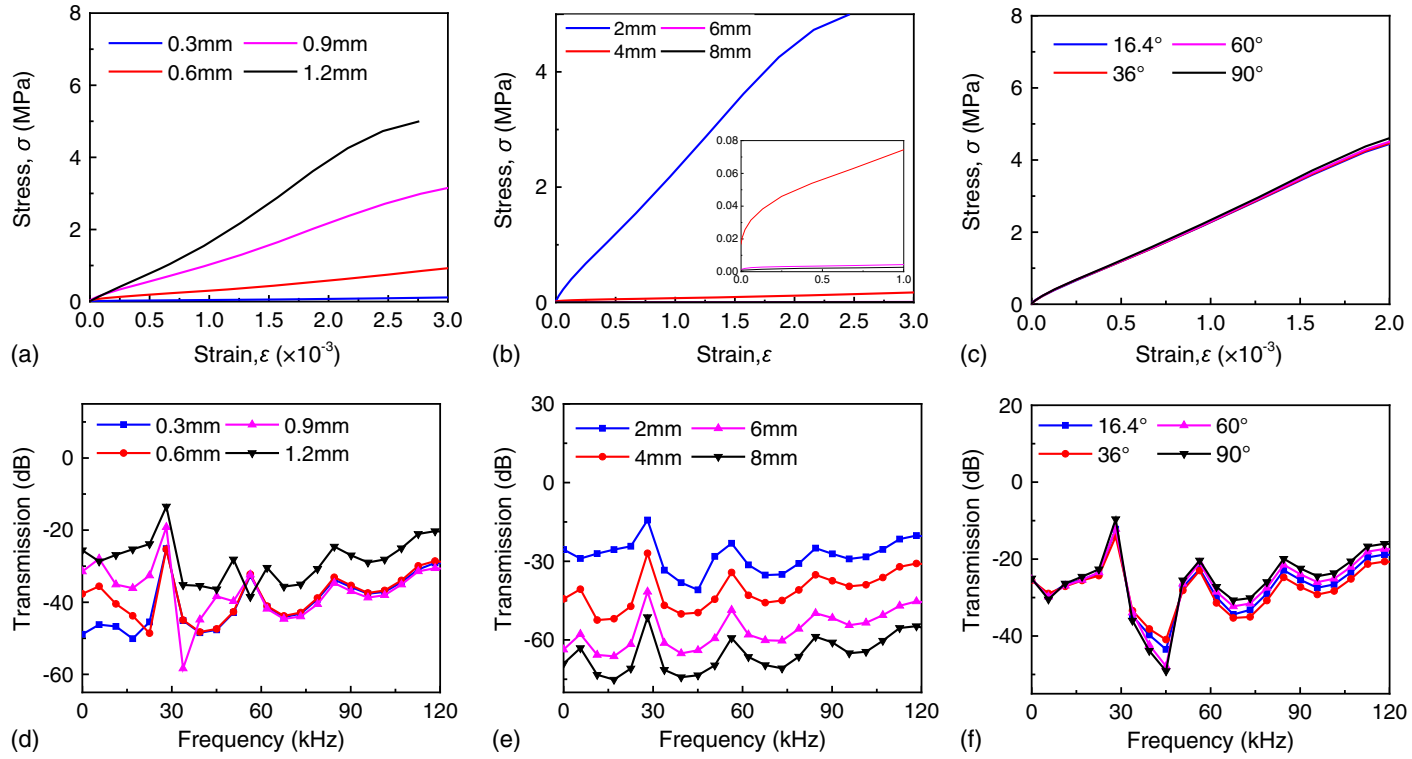

Fig. 6. (a and b) Stress–strain curves with fiber amplitude A ($A = 0$ if the fibers are straight); (c and d) corresponding stress-wave transmission of a herringbone specimen with different geometries with wavelength λ; and (e and f) helicoidal angle α.

Moreover, transmission within the four band gaps decreased with the fiber wavelength λ. Therefore, wave filtering of elastic waves increased with λ. Notably, the effect of helicoid angle on the dynamic responses of the herringbone structure was negligible, as shown in Fig. 6(c).

Effects of Fiber Architecture

To elucidate the toughening mechanism of the dactyl club, the Bouligand structure of the inner periodic region, the herringbone structure of the outer impact region, and a combined structure were simulated and compared, as shown in Fig. 7(a). The combined

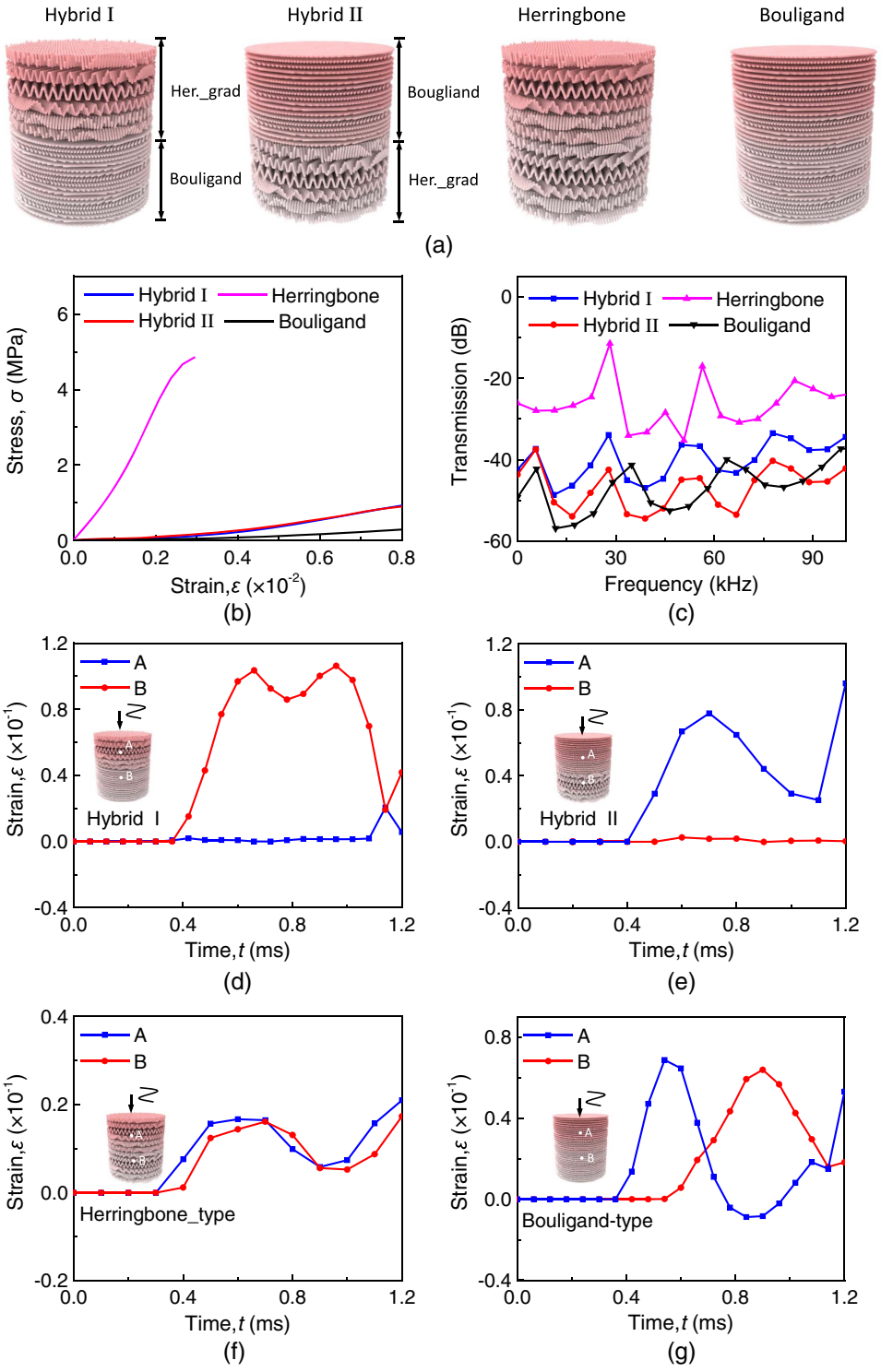

Fig. 7. (a) Specimens with different fiber architectures; (b) comparison of stress–strain curves; (c) corresponding stress-wave transmission through four types of architectures; and (d–g) stress-wave propagation in each type of specimen. Plot (d) shows Hybrid I, plot (e) shows Hybrid II, plot (f) shows the Herringbone-type, and plot (g) shows the Bouligand-type. The stress wave was extracted, respectively, from the Bouligand and herringbone regions in Hybrid-type structures.

J. Aerosp. Eng., 2022, 35(5): 04022056

structure was stiffer than the uniform one because the sinusoidally periodic fibers of the Herringbone_grad structure was more effective at resisting vertical deformation than the horizontal fibers of the Bouligand structure. In addition, as shown in Fig. 7(c), the wave-filtering effect varied with fiber architecture. The herringbone structure had the weakest wave-filtering effect. Compared with the Bouligand structure, transmission within the band gaps of the Hybrid I structure increased, indicating that the wave-filtering effect was weaker in the herringbone structure. Although the Hybrid II structure was comparable to the Bouligand structure, the band gaps of the former existed at lower frequencies. From the perspective of impact dynamics, the herringbone structure should be employed to resist vertical deformation, whereas the Bouligand structure is suitable for wave filtering at a specific frequency range. Therefore, a hybrid structure (herringbone and Bouligand) in the dactyl club of mantis shrimps can resist high-strain-rate impacts.

To study wave propagation in each fiber architecture, the stress wave passing through two selected points located on the surface of each sample was extracted [Figs. 7(d–g)]. For the combined structures (Hybrid I and Hybrid II), the stress wave was weak in the Herringbone_grad region and became stronger in the Bouligand region. Therefore, sinusoidal fibers could mitigate high-peak waves, irrespective of the order of combination [Figs. 7(d and e)]. For the Herringbone-type and Bouligand-type structures [Figs. 7(f and g)], the stress wave resembled a soliton with one hump, and its amplitude varied negligibly as it passed from Point A to Point B. Moreover, the wave speed in the Herringbone-type structure was larger than that in the Bouligand-type structure, suggesting that uniform stress was established more quickly in the former fiber architecture.

To further analyze the stress distribution, the Von Mises stress contours of the first six layers during wave propagation are compared in Fig. 8. Stress distribution was more uniform in the Herringbone-type region than in the Bouligand-type region of the combined structure. Therefore, the sinusoidally periodic fiber structure on the outer surface can mitigate the impact stress wave and trigger uniform stress redistribution, which protects the stomatopod when its appendage impacts hard-shell preys.

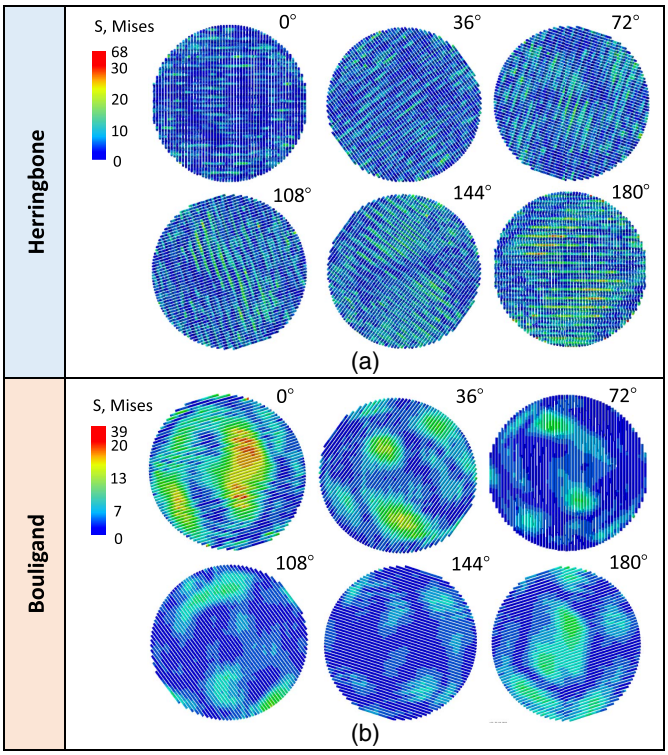

Fig. 8. Stress distribution comparison of the first six layers, respectively, from (a) Herringbone-type; and (b) Bouligand-type materials. The helicoidal angle of each layer is labeled.

Conclusion

The fiber architectures in the stomatopod dactyl club played an important role in the impact resistance and damage tolerance of the dactyl club. Herringbone composites based on the fiber architecture in the impact region of the dactyl club were printed, and their dynamic behavior under different strain rates were investigated. The main results can be summarized as follows:

- Herringbone composites exhibited a more uniform stress distribution than the Bouligand-type composites because the sinusoidally periodic fibers were flattened during compression. Herringbone composites also possessed greater energy-absorption capability with postponed densification strain. Moreover, materials with the herringbone architecture were less sensitive to strain rate. However, the fiber amplitude and wavelength would affect material stiffness and wave filtering.
- The sinusoidally periodic fiber architecture on the outer surface can mitigate the impact stress wave, whereas the Bouligand-type structure can filter waves at a specific frequency range. Thus, a multiregion architecture formed by combining the outer herringbone structure with the inner Bouligand-type structure provides effective impact resistance and damage tolerance for the appendage of the mantis shrimp.

In this study, the toughening mechanism of the composites was correlated with the fiber patterns of different regions. The results would shed light on the design of impact-resistant bioinspired composite materials.

Data Availability Statement

Some or all data, models, or code that support the findings of this study are available from the corresponding author upon reasonable request.

Acknowledgments

S. Yin is grateful for the financial support from Natural Science Foundation of China (No. 12172025), the Open Research Fund Project of the State Key Laboratory for Advanced Forming Technology & Equipment (SKL2019001), Beihang-CAIP Lightweight Research Institute, and the Fundamental Research Funds of the Central Universities, Beihang University.

Supplemental Materials

Figs. S1–S4 and Table S1 are available online in the ASCE Library (www.ascelibrary.org).

References

Agarwal, K., Y. Zhou, H. P. Anwar Ali, I. Radchenko, A. Baji, and A. S. Budiman. 2018. "Additive manufacturing enabled by electrospinning for tougher bio-inspired materials." *Adv. Mater. Sci. Eng.* 2018 (Jan): 1–9. https://doi.org/10.1155/2018/8460751.

Amini, S., A. Masic, L. Bertinetti, J. S. Teguh, J. S. Herrin, X. Zhu, and H. Su. 2014. "Textured fluorapatite bonded to calcium sulphate strengthen stomatopod raptorial appendages." *Nat. Commun.* 5 (1): 1–12. https://doi.org/10.1038/ncomms4187.

Amini, S., M. Tadayon, S. Idapalapati, and A. Miserez. 2015. "The role of quasi-plasticity in the extreme contact damage tolerance of the stomatopod dactyl club." *Nat. Mater.* 14 (9): 943–950. https://doi.org/10.1038/nmat4309.

Burrows, M. J. Z. F. V. P. 1969. "The mechanics and neural control of the prey capture strike in the mantid shrimps *Squilla* and *Hemisquilla*." *Z. Vergl. Physiol.* 62 (10): 361–381. https://doi.org/10.1007/BF00299261.

Caldwell, R. L., and H. J. N. Dingle. 1975. "Ecology and evolution of agonistic behavior in stomatopods." *Naturwissenschaften* 62 (5): 214–222. https://doi.org/10.1007/BF00603166.

Dunlop, J. W., and P. Fratzl. 2010. "Biological composites." *Ann. Rev. Mater. Res.* 40 (Aug): 1–24. https://doi.org/10.1146/annurev-matsci-070909-104421.

Fabritius, H. O., C. Sachs, P. R. Triguero, and D. Raabe. 2009. "Influence of structural principles on the mechanics of a biological fiber-based composite material with hierarchical organization: The exoskeleton of the lobster *Homarus americanus*." *Adv. Mater.* 21 (4): 391–400. https://doi.org/10.1002/adma.200801219.

Grunenfelder, L. K., G. Milliron, S. Herrera, I. Gallana, N. Yaraghi, N. Hughes, and K. Evans-Lutterodt. 2018. "Ecologically driven ultrastructural and hydrodynamic designs in stomatopod cuticles." *Adv. Mater.* 30 (9): 1705295. https://doi.org/10.1002/adma.201705295.

Grunenfelder, L. K., N. Suksangpanya, C. Salinas, G. Milliron, N. Yaraghi, S. Herrera, and K. Evans-Lutterodt. 2014. "Bio-inspired impact-resistant composites." *Acta Biomater.* 10 (9): 3997–4008. https://doi.org/10.1016/j.actbio.2014.03.022.

Gu, G. X., M. Takaffoli, A. J. Hsieh, and M. Buehler. 2016. "Biomimetic additive manufactured polymer composites for improved impact resistance." *Extreme Mech. Lett.* 9 (Dec): 317–323. https://doi.org/10.1016/j.eml.2016.09.006.

Guarin-Zapata, N., J. Gomez, N. Yaraghi, D. Kisailus, and P. D. Zavattieri. 2015. "Shear wave filtering in naturally-occurring Bouligand structures." *Acta Biomater.* 23 (Sep): 11–20. https://doi.org/10.1016/j.actbio.2015.04.039.

Guo, W., Y. Huang, R. O. Ritchie, and S. Yin. 2021. "Dissipative dual-phase mechanical metamaterial composites via architectural design." *Extreme Mech. Lett.* 48 (Oct): 101442. https://doi.org/10.1016/j.eml.2021.101442.

Han, Q., S. Shi, Z. Liu, Z. Han, S. Niu, J. Zhang, and H. Qin. 2020. "Study on impact resistance behaviors of a novel composite laminate with basalt fiber for helical-sinusoidal bionic structure of dactyl club of mantis shrimp." *Composites, Part B* 191 (Jun): 107976. https://doi.org/10.1016/j.compositesb.2020.107976.

Meyers, M. A., P. Y. Chen, A. Y. M. Lin, and Y. Seki. 2008. "Biological materials: Structure and mechanical properties." *Prog. Mater. Sci.* 53 (1): 1–206. https://doi.org/10.1016/j.pmatsci.2007.05.002.

Patek, S., and R. Caldwell. 2005. "Extreme impact and cavitation forces of a biological hammer: Strike forces of the peacock mantis shrimp *Odontodactylus scyllarus*." *J. Exp. Biol.* 208 (19): 3655–3664. https://doi.org/10.1242/jeb.01831.

Patek, S. N., W. Korff, and R. Caldwell. 2004. "Deadly strike mechanism of a mantis shrimp." *Nature* 428 (6985): 819–820. https://doi.org/10.1038/428819a.

Quan, H., W. Yang, Z. Tang, R. O. Ritchie, and M. A. Meyers. 2020. "Active defense mechanisms of thorny catfish." *Mater. Today* 38 (4): 35–48. https://doi.org/10.1016/j.mattod.2020.04.028.

Ren, L., X. Zhou, Q. Liu, Y. Liang, Z. Song, B. Zhang, and B. Li. 2018. "3D magnetic printing of bio-inspired composites with tunable mechanical properties." *J. Mater. Sci.* 53 (5): 14274–14286. https://doi.org/10.1007/s10853-018-2447-5.

Rosenberg, M. S. J. 2002. "Fiddler crab claw shape variation: A geometric morphometric analysis across the genus *Uca* (Crustacea: *Brachyura: Ocypodidae*)." *Biol. J. Linn. Soc.* 75 (2): 147–162. https://doi.org/10.1046/j.1095-8312.2002.00012.x.

Weaver, J. C., G. W. Milliron, A. Miserez, K. Evans-Lutterodt, S. Herrera, I. Gallana, and W. J. Mershon. 2012. "The stomatopod dactyl club: A formidable damage-tolerant biological hammer." *Science* 336 (6086): 1275–1280. https://doi.org/10.1126/science.1218764.

Wu, K., Z. Song, S. Zhang, Y. Ni, S. Cai, X. Gong, and L. He. 2020. "Discontinuous fibrous Bouligand architecture enabling formidable fracture resistance with crack orientation insensitivity." *Proc. Natl. Acad. Sci. U.S.A.* 117 (27): 15465–15472. https://doi.org/10.1073/pnas.2000639117.

Wu, Q., A. Vaziri, M. E. Asl, R. Ghosh, Y. Gao, X. Wei, and L. Ma. 2019. "Lattice materials with pyramidal hierarchy: Systematic analysis and three dimensional failure mechanism maps." *J. Mech. Phys. Solids* 125 (4): 112–144. https://doi.org/10.1016/j.jmps.2018.12.006.

Yang, X., J. Ma, Y. Shi, Y. Sun, and J. Yang. 2017. "Crashworthiness investigation of the bio-inspired bi-directionally corrugated core sandwich panel under quasi-static crushing load." *Mater. Des.* 135 (Sep): 275–290. https://doi.org/10.1016/j.matdes.2017.09.040.

Yaraghi, N. A., N. Guarín-Zapata, L. K. Grunenfelder, E. Hintsala, S. Bhowmick, J. M. Hiller, and M. Betts. 2016a. "Biocomposites: A sinusoidally architected helicoidal biocomposite." *Adv. Mater.* 28 (2): 6769. https://doi.org/10.1002/adma.201670219.

Yaraghi, N. A., N. Guarin-Zapata, L. K. Grunenfelder, E. Hintsala, S. Bhowmick, J. M. Hiller, and M. Betts. 2016b. "A sinusoidally architected helicoidal biocomposite." *Adv. Mater.* 28 (32): 6835–6844. https://doi.org/10.1002/adma.201600786.

Yin, S., H. Chen, R. Yang, Q. He, D. Chen, L. Ye, and Y. W. Mai. 2020. "Tough nature-inspired helicoidal composites with printing-induced voids." *Cell Rep. Phys. Sci.* 1 (7): 100109. https://doi.org/10.1016/j.xcrp.2020.100109.

Yin, S., W. Guo, H. Wang, Y. Huang, R. Yang, Z. Hu, and D. Chen. 2021a. "Strong and tough bioinspired additive-manufactured dual-phase mechanical metamaterial composites." *J. Mech. Phys. Solids* 149 (2): 104341. https://doi.org/10.1016/j.jmps.2021.104341.

Yin, S., J. Li, H. Chen, R. O. Ritchie, and J. Xu. 2018. "Design and strengthening mechanisms in hierarchical architected materials processed using additive manufacturing." *Int. J. Mech. Sci.* 149 (3): 150–163. https://doi.org/10.1016/j.ijmecsci.2018.09.038.

Yin, S., H. Wang, J. Hu, Y. Wu, Y. Wang, S. Wu, and J. Xu. 2019. "Fabrication and anti-crushing performance of hollow honeytubes." *Composites, Part B* 179 (Feb): 107522. https://doi.org/10.1016/j.compositesb.2019.107522.

Yin, S., L. Wu, and S. Nutt. 2013. "Stretch–bend-hybrid hierarchical composite pyramidal lattice cores." *Compos. Struct.* 98 (Apr): 153–159. https://doi.org/10.1016/j.compstruct.2012.11.004.

Yin, S., R. Yang, Y. Huang, W. Guo, D. Chen, W. Zhang, and M. Ren. 2021b. "Toughening mechanism of coelacanth-fish-inspired double-helicoidal composites." *Compos. Sci. Technol.* 205 (Mar): 108650. https://doi.org/10.1016/j.compscitech.2021.108650.

Zaheri, A., J. S. Fenner, B. P. Russell, D. Restrepo, M. Daly, D. Wang, and C. Hayashi. 2018. "Revealing the mechanics of helicoidal composites through additive manufacturing and beetle developmental stage analysis." *Adv. Funct. Mater.* 28 (1): 1803073. https://doi.org/10.1002/adfm.201803073.